On the potential of meta-poro-elastic systems with mass inclusions to achieve broadband near-perfect absorption coefficient

S Ahsani, R F Boukadia, C Droz, T G Zieliński, Ł Jankowski, C Claeys, W Desmet, E Deckers

On the potential of meta-poro-elastic systems with mass inclusions to achieve broadband near-perfect absorption coefficient

S. Ahsani [1,2], **R.F. Boukadia** [1,2,3], **C. Droz** [1,2], **T. G. Zieliński** [5], **Ł. Jankowski** [5], **C. Claeys** [1,2], **W. Desmet** [1,2], **E. Deckers** [2,4]
[1] KU Leuven, Department of Mechanical Engineering,Division LMSD
Celestijnenlaan 300, B-3001, Heverlee, Belgium
e-mail: **sepide.ahsani@kuleuven.be**

[2] DMMS Lab, Flanders Make
Heverlee, Belgium

[3] École Centrale de Lyon
36 Avenue Guy de Collongue, 69134 Écully Cedex, France

[4] KU Leuven, Campus Diepenbeek Department, Mechanical Engineering
Wetenschapspark 27, 3590 Diepenbeek, Belgium

[5] Institute of Fundamental Technological Research, Polish Academy of Sciences,
ul. Swietokrzyska 21, 00-049 Warszawa, Poland

Abstract
This paper discusses the potential of meta-poro-elastic systems with small mass inclusions to create broadband sound absorption performance under the quarter-wavelength limit. A first feasibility study is done to evaluate whether embedding small mass inclusions in specific types of foam can lead to near-perfect absorption at tuned frequencies. This paper includes an optimization routine to find the material properties that maximize the losses due to the mass inclusion such that a near-perfect/perfect absorption coefficient can be achieved at specified frequencies. The near-perfect absorption is due to the mass-spring effect, which leads to an increase in the viscous loss. Therefore, it is efficient in the viscous regime. The well-known critical frequency, which depends on the porosity and flow resistivity of the material, is commonly used as a criteria to distinguish the viscous regime from the inertial regime. However, for the types of foam of interest to this work, the value of critical frequency is below the mass-spring resonance frequency. Hence, the inverse quality factor is used to provides a more accurate estimation on the frequency at which the transition from the viscous regime to the inertial regime.

1 Introduction

Poro-elastic materials are commonly used in many industries as a sound-absorbing treatment. However, their efficiency is limited to mid- and high-frequencies, where a thickness of quarter-wavelength would not result in bulky treatments. Therefore, many research efforts in the recent years focused on improving the low-frequency behavior of poro-elastic materials by embedding different types of inclusion in the material. Groby et al. [1] investigated the modal behavior of a porous layer with low/high contrast inclusions. They showed that high contrast inclusions can modify the mode of the layer with a frequency offset from the natural frequency of the layer. This offset depends on the spacing between the inclusions and the inclusion geometry. They explained that the modified mode corresponds to evanescent waves in the ambient fluid and

propagative ones in the porous layer, which leads to energy entrapment in the porous layer and consequently an increase in the absorption. Another effect exists that leads to energy entrapment in the porous layer, which is known as the trapped mode effect [2]. Groby et al. [3] showed that using a rigid inclusion of comparable size as the acoustic wavelength in a rigid frame foam, the energy can be trapped between the rigid wall and the inclusion leading to a perfect absorption above the decoupling frequecy i.e. in the inertial regime. Weisser et al. [4] investigated the effect of elastic inclusions in a poro-elastic layer. They considered two types of inclusions i.e. a soft and a hard elastic inclusion with comparable size to the acoustic wavelength and a very thin rubber shell ring. The former showed the same behavior as the rigid inclusion leading to a perfect absorption using the trapped mode effect. The latter showed absorption improvement at the flexural mode of the ring in the viscous regime. In [5] the effect of periodic point mass inclusions in a poro-elastic layer was investigated numerically. The investigation showed that the sound absorption performance can be improved by the so-called mass-spring effect, where the foam under the mass is considered to be the spring. It was shown that the resonance frequency of the mass-spring system depends on the mass and location of the inclusion. The mass-spring effect was observed and confirmed experimentally in acoustic blankets with randomly placed mass inclusions [6] in the context of transmission loss improvement.

These works show the potential of meta-poro-elastic systems to improve the absorption coefficient below the decoupling frequency by exploiting the resonant behavior being the mode of the inclusion or the mass-spring effect. It is shown in [7] that the amount of the absorption enhancement due to the mass-spring effect is proportional with the viscous coupling coefficient [8, 9], i.e. viscous characteristic length and the flow resisitivity of the poro-elastic layer. Therefore, an optimization routine is used in this paper to find material properties that can lead to a perfect absorption using the mass-spring effect. On the other hand, it is known that the number of resonance frequencies of a mass-spring system is limited to the number of degrees of freedom (DOFs) of the system. In other word, the peaks in the absorption coefficient is rather narrow and limited to DOFs of the mass-spring system. In this paper the potential of achieving a broadband perfect absorption by creating a super-cell [10] with multiple mass inclusions (a multi-DOF mass-spring system) tuned at different frequencies. Additionally, a detailed discussion is given on the decoupling frequency since the efficiency of the mass-spring effect is strongly connected to the viscous losses.

This paper is structured as follows. Section 2 details the configurations studied in the paper and the modeling technique used to calculate the sound absorption of the system. Section 3 focuses on the potential of the meta-poro-elastic system to achieve broadband near-perfect/perfect absorption using the mass-spring effect. Firstly, the sound absorbing behaviors of a homogeneous layer and a reference meta-poro-elastic layer are discussed briefly. Secondly, the optimization routine for a periodic unit cell (PUC) with single inclusion and a super-cell (with multiple inclusions) is explained. Thirdly, the criteria to distinguish the viscous regime from the inertial regime is explained. The paper is concluded in the section 4.

2 Problem description

This section consists of three parts. The first part describes the problem configuration. The second part briefly explains the material modeling used in this paper. The third part details the absorption coeffcient calculation.

2.1 Problem configuration

In this paper an infinite 2D poro-elastic layer with and without inclusions is considered, see Figure 1. The structure is modeled as a 2D plain strain problem in the $x-y$ plane. The unbounded acoustic domain and the poro-elastic domain are denoted by Ω_a and Ω_p, respectively. The problem is periodic in the $x-$direction with a PUC characteristic length of l_x in case of poro-elastic layer with a single inclusion per PUC, see Figure 1(b) and L_x in case of super-cell with multiple inclusions, see Figure 1(c). The layer is rigidly backed and excited by an acoustic plane wave with normal angle of incidence. The meta-poro-elastic systems are obtained by introducing one inclusion at point (x_0, y_0) or multiple inclusions at different positions (x_i, y_i).

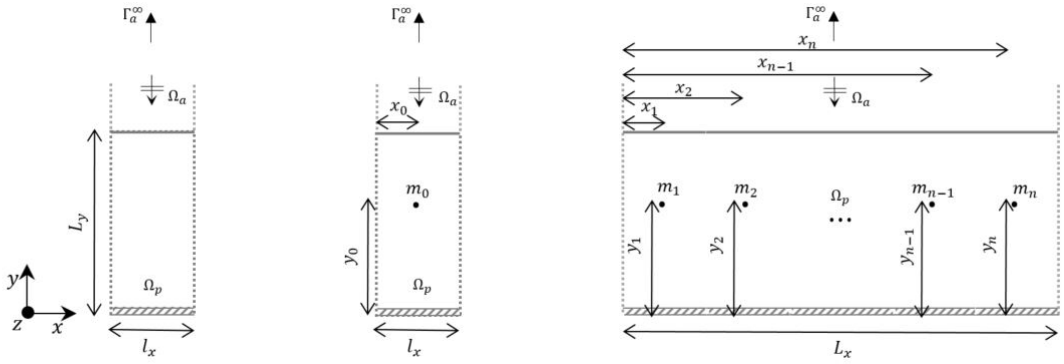

(a) (b) (c)

Figure 1: Schematic view of the problem configurations:(a) Poro-elastic layer (b) Single inclusion meta-poro-elastic layer (c) Periodic super-cell composed of n unit cells.

2.2 Modeling technique

The Helmholtz equation [11] is used to model the steady-state behavior of the semi-infinite acoustic domain. The Biot-Allard model [12, 13, 14, 15, 16] is used for the poro-elastic domain in order to consider the frame vibration and all the energy dissipation mechanisms, i.e. the viscous, thermal, and structural effects [17]. The mixed $\mathbf{u} - p$ formulation [18, 19] is used, where the field variables are the solid-phase displacements and the pore-fluid pressure. The coupling between the acoustic and poro-elastic domain [20] is considered by (i) applying the continuity of the pressure at the interface (ii) imposing the pressure loading on the solid phase, and the structural acceleration on the acoustic domain pressure due to the poro-elastic solid phase. Readers are referred to [8] for the description of these coupling conditions. Moreover, the acoustic pressure is decomposed in terms of propagative Bloch modes [21] at the radiating boundary to account for the non-reflecting boundary at the unbounded interface of the acoustic domain. Additionally, the solid phase displacement in $y-$direction is constrained at the base to model the connection to the rigid wall.

Periodic field variables are considered for the acoustic domain (Ω_a) and the poro-elastic domain (Ω_p) to ensure the Floquet-Bloch relation [22, 23]:

$$W(\mathbf{x} + \mathbf{d}) = W(\mathbf{x}) \exp\left(\mathrm{i}\tilde{\mathbf{k}} \cdot \mathbf{d}\right), \tag{1}$$

where $\mathbf{d} = \{d_x, 0, 0\}$ is the spatial periodicity vector, in which $d_x = l_x$ for the single inclusion meta-poro-elastic case and $d_x = L_x$ for the super-cell case. Moreover, $\tilde{\mathbf{k}} = \{\tilde{k}_x, 0, 0\}$ is the trace wavenumber of the incident acoustic plane wave. Furthermore, the inclusion is considered as concentrated point mass (m_i), where only its inertial contribution is taken into account [5]. The Finite Element Method (FEM) is used to solve the problem.

2.3 Absorption coefficient calculation

In this work, the performance of the proposed systems are evaluated in terms of its sound absorption coefficient, which is calculated using the average acoustic impedance ($Z = p_t/v$) at the interface between the acoustic and poro-elastic domains. In this definition, p_t is the total acoustic pressure and v is the velocity of the propagative acoustic wave at the interface. The system sound absorption coefficient under the plane acoustic wave excitation with normal incidence angle is determined as follows:

$$\alpha = 1 - \left|\frac{Z - Z_0}{Z + Z_0}\right|^2, \tag{2}$$

where $Z_0 = \rho_0 c_0$ is the characteristic impedance of the air with ρ_0 and c_0 being the air density and sound speed respectively. In this paper, the absorption coefficient is decomposed in terms of viscous and struc-

tural energy dissipation mechanisms, such that the resonance frequency of the frame and the inclusion or inclusions can be identified. The mathematical description of this decomposition can be found in [17].

3 Results and discussion

This section consists of three parts. Firstly, the design of the proposed meta-poro-elastic configuration as well as its specifications are detailed. This design is considered as the reference case. Secondly, the sound absorption of the reference case is evaluated and is compared to the homogeneous layer of the same poro-elastic material. Thirdly, an optimization routine is detailed and the results of the optimization of the meta-poro-elastic system with a single inclusion and the super-cell with multiple inclusions are evaluated. Finally, the efficiency of the mass-spring effect in the viscous regime is discussed in detail.

3.1 Meta-poro-elastic system design

Two cases are considered in this part. The first case consists of a homogeneous polyurethane (PU) foam layer of thickness $L_y = 24\ \mathrm{mm}$. The material properties of the PU foam are shown in Table 1 , where E, η are the elastic modulus and loss factor of the frame, ν is the bulk Poisson ratio, ρ_1 is the bulk density, ϕ is the porosity, α_∞ is the tortuosity, Λ, Λ' are the viscous and thermal characteristic lengths, and σ is the airflow resistivity. These parameters are taken from [5].

The second case is the proposed design of a meta-poro-elastic system with a concentrated mass of $m_0 = 0.0039\ kg$ equivalent to the mass by a rod steel inclusion of radius $r = 0.4\ mm$ embedded in the homogeneous layer. The location of this idealized point mass is $(x_0, y_0) = (4, 12)$ mm. The proposed design is periodic in the $x-$direction with a PUC characteristic length of $l_x = 8$ mm. The acoustic and poro-elastic domains are discretized using 710 TRI6 elements leading to a total of 4142 DOFs.

Table 1: The Biot parameters of the PU foam [5].

E (kPa)	η (-)	ν (-)	ρ_1 (kg/m^3)	ϕ (-)	α_∞	Λ (μm)	Λ' (μm)	σ (Pa·s/m^4)
143	0.055	0.3	31	0.97	2.52	37	119	87000

3.2 Sound absorption of the reference meta-poro-elastic system

The total sound absorption coefficients and the decomposed absorption coefficients in terms of viscous and structural losses of the homogeneous layer and the reference meta-poro-elastic case are shown in Figure 2. The resonance frequency of the frame [14] for the homogeneous case is observed at 820 Hz. This frequency corresponds to a peak in the structural losses. At the same time, two peaks in the structural losses are observed for the reference meta-poro-elastic case at 520 Hz (resonance frequency of the inclusion) and 1480 Hz (modified resonance frequency of the frame). The first peak is induced by the mass-spring effect [7], while the second one is induced by the modified mode effect [1]. The resonance frequency of the inclusion depends on the poro-elastic material properties as well as the vertical position and the mass of the inclusion, while the modified mode frequency of the frame depends on the foam properties, PUC characteristic length, and the spacing between the inclusions.

Moreover, the meta-poro-elastic system shows an improved absorption behavior, for example at $f = 770$ Hz from $\alpha = 0.23$ to $\alpha = 0.65$, as compared to the homogeneous case. But this improvement is far from a perfect absorption behavior. The latter gives the motivation to use an optimization routine such that the energy losses due to the mass-spring effect are maximized.

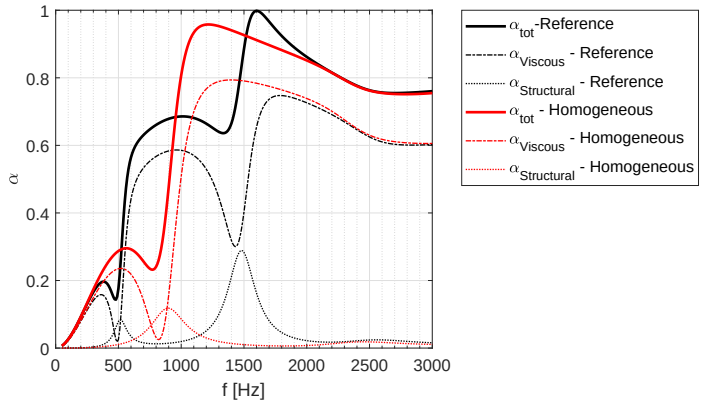

Figure 2: Total and partial absorption coefficients for the homogeneous layer and the reference (i.e. not optimised) meta-poro-elastic case.

3.3 Optimization of the meta-poro-elastic system

A pattern search algorithm [24] is used for the optimization of the meta-poro-elastic system. In the optimization routine the horizontal position of the inclusion (x_0), the added mass (m_0), the PUC characteristic length (l_x), and the poro-elastic layer thickness (L_y) are kept identical as the reference case. The design space consists of foam material properties ($\sigma,\ \Lambda,\ \Lambda',\ \rho_1,\ E,\ \eta$) and the vertical position of the inclusion i.e. y_0. All the design parameters are normalized using scale factors such that the relative change in all of them is of the same order at each iteration step. Moreover, a mesh expansion factor of 4, and a mesh contraction factor of 2 is chosen. The target function is defined as:

$$f_p = \sum_{i=1}^{i=m} (1 - a_i \alpha_i)^2, \tag{3}$$

where m is the number of tuned frequencies, α_i is the value of absorption coefficient at each tuned frequency, and a_i is the correction factor for each value of absorption coefficient defined as follows:

$$a_i = \begin{cases} 0 & \alpha_i < 0.8 \\ 1 & \alpha_i \geq 0.8. \end{cases} \tag{4}$$

This definition is used such that the convergence of the optimization to a global minimum is ensured. The considered tuned frequency for the optimization of the PUC with single inclusion is 700 Hz. The lower bound (LB), upper bound (UB), and the converged values (CV) of the design space parameters are summarized in Table 2.

Table 2: The upper bound, lower bound, and the converged values of the design space parameters.

	E (kPa)	η	ρ_1 (kg/m^3)	Λ (μm)	Λ' (μm)	σ (kPa·s/m^4)	y_0(mm)
LB	3	0.01	10	1	1	1	0
UB	200	0.1	90	300	300	90	23
CV	159.62	0.0105	37.09	7.28	1	1.012	12.5

The total and partial absorption coefficients of the optimized configuration are shown in Figure 3. Additionally, the total absorption coefficient of a homogeneous layer of the foam with optimized material properties is calculated and compared to optimized meta-poro-elastic case. It can be seen that the optimized case shows perfect absorption at the tuned frequency of 700 Hz due to the mass-spring effect. Moreover, it is apparent that the viscous losses are very high at that frequency. There are two reasons behind such behavior. Firstly, the resonating inclusion excites the frame to move out-of-phase with respect to the fluid phase. Secondly, the

optimized case has a very low viscous characteristic length, which corresponds to a high amount of viscous loss if the motions of the solid frame and fluid in the pores are out of phase. On the other hand, it can be seen that this type of material shows poor performance at frequencies where the frame is not in motion, i.e. frequencies outside the modified mode of the frame and the resonance of the inclusion. This raises the following question: can broadband perfect absorption be achieved for a super-cell with multiple inclusions tuned at different frequencies? This forms the topic of the next section.

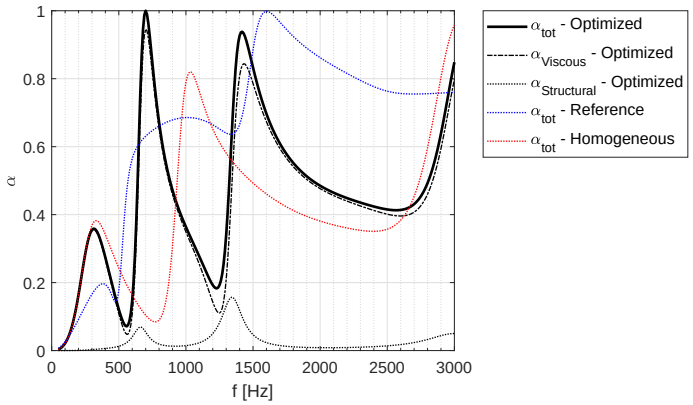

Figure 3: Total and partial absorption coefficients for the homogeneous layer, the reference (i.e. not optimized) meta-poro-elastic, and for the optimized case.

3.4 Optimization of the super-cell meta-poro-elastic system

In this part, the same optimization routine is used for the super-cell layer shown in Figure 1(c). A super-cell with $n = 4$ inclusions is considered. The optimized material properties obtained in section 3.3 are used, and the layer thickness (L_y) is the same as in the reference case. The design space consists of the position of four inclusions, i.e. (x_i, y_i) for $i = 1, ..., 4$, and the PUC characteristic length, i.e. L_x. Five tuning frequencies are considered in the optimization of the super-cell, viz. $f = 700,\ 900,\ 1100,\ 1300,\ 1500$ Hz. The lower bound (LB) and upper bound (UB) for the horizontal position, vertical position, and PUC characteristic length in millimeters are: $[\mathrm{LB}_{x_i}, \mathrm{UB}_{x_i}] = [1, 20l_x]$, $[\mathrm{LB}_{y_i}, \mathrm{UB}_{y_i}] = [1, 23]$, and $[\mathrm{LB}_{L_x}, \mathrm{UB}_{L_x}] = [l_x, 20l_x]$. The converged values (CV) of the design space parameters and the resulting configuration are given in Table 3.

Table 3: The schematic view of the optimized super-cell configuration with four inclusions and the converged values of the design space parameters of the super-cell optimization.

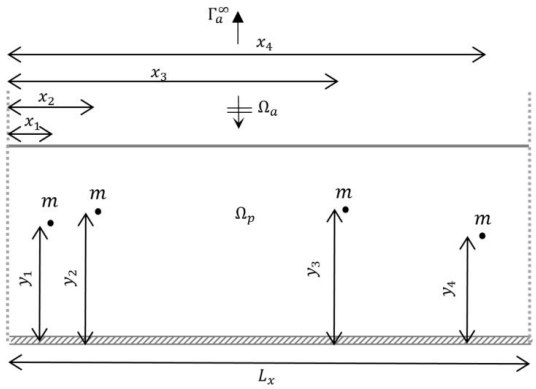

	CV (mm)
(x_1, y_1)	$(0.69l_x, 14)$
(x_2, y_2)	$(1.31l_x, 16)$
(x_3, y_3)	$(5l_x, 16.5)$
(x_4, y_4)	$(7.22l_x, 13)$
L_x	$7.875l_x$

The total and partial (decomposed) absorption coefficients of the optimized super-cell configuration are shown in Figure 4. Five near-perfect absorption peaks around the tuned frequencies are present. Four peaks correspond to the four inclusion resonances and the additional peak corresponds to the modified mode of the

frame. The converged values given in Table 3 show that each inclusion can be tuned to a different frequency by changing its position inside the super-cell. The super-cell characteristic length (L_x) is also an important factor, since this value influences strongly the spacing between the inclusions within the super-cell. Figure 4 shows clearly the potential of such super-cell meta-poro-elastic systems with mass inclusions to create an enhanced absorption in a tuned wide-band frequency range.

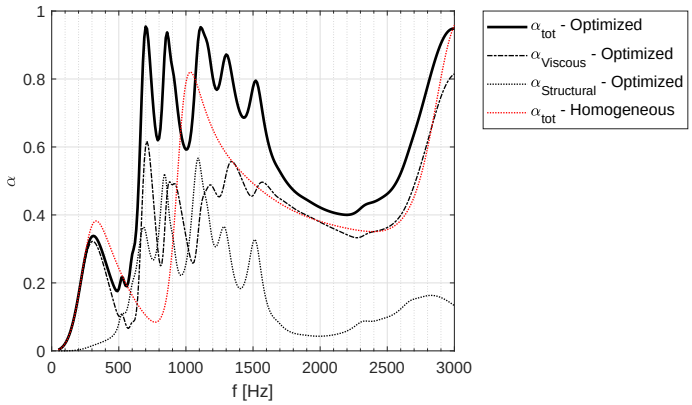

Figure 4: Total and partial absorption coefficients for the homogeneous layer and the optimized case of the super-cell layer.

3.5 Discussion on the decoupling frequency

The decoupling frequency corresponds to the frequency at which the two phases of the poro-elastic material decouple and the frame acts as rigid. Above this frequency the energy losses are mainly due to inertial effects, while below this frequency energy is dissipated mainly through viscous effects. This frequency, known in literature as the critical frequency, is commonly defined as [9]:

$$f_c = \frac{\phi\sigma}{2\pi\rho_0}. \tag{5}$$

The critical frequency for the optimized foam of single inclusion PUC is $f_c = 129$ Hz. Moreover, it was shown previously that at 700 Hz a perfect absorption coefficient can be achieved due to the mass-spring effect. This seems to contradict the assumption that the mass-spring effect is efficient in the viscous regime, since 700 Hz is above the critical frequency for the optimized foam. Therefore, the decoupling frequency is reevaluated using the inverse quality factor [25]:

$$Q^{-1} = \left| \frac{Im(k_{Li})}{Re(k_{Li})} \right| \qquad (i = 1, 2), \tag{6}$$

where k_{Li} $(i = 1, 2)$ is the wavenumber associated to the slow ($L1$), and fast ($L2$) longitudinal waves propagating in the poro-elastic layer. The inverse quality factor measures the amount of damped energy with respected to the total wave energy for each wave type. Therefore, the inverse quality factor value for $L1$ is high at low frequencies since this wave corresponds to the relative motion of the two phases. Its value decreases around the decoupling frequency, where the energy dissipation is mainly due to the inertial effect rather than viscous effect. At the same time, the value of the inverse quality factor for $L2$ starts to increase and reaches a maximum at the decoupling frequency. Above the decoupling frequency its value drops down reaching to zero at high frequencies. Therefore, the peak in the inverse quality factor for L2 can be used as a criterium to define the decoupling frequency. The inverse quality factor of the two longitudinal waves of a homogeneous layer of the optimized foam are shown in Figure 5 where the frequency range of the study is normalized with respect to the critical frequency (f_c), computed using Eq. (5), for a better comparison. It can be seen that for the optimized foam, the transition from viscous regime to inertial regime occurs around

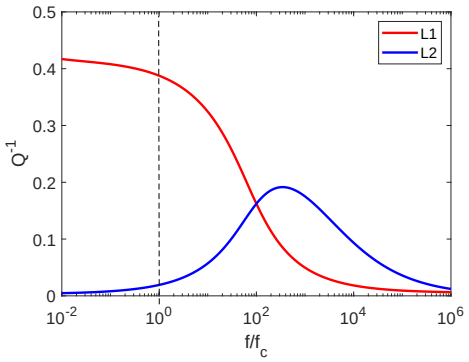

Figure 5: Inverse quality factor of optimized foam.

$\frac{f}{f_c} \approx 200$. This is due to the fact that the critical frequency (f_c) definition does not consider the viscous characteristic length, which also contributes to the amount of viscous losses. The optimized foam has a very low viscous characteristic length leading to a very high viscous loss in case of out-of-phase motion of the two phases.

To further clarify that the decoupling of the fluid and solid phase for the optimized foam occurs at a much higher frequency as compared to the critical frequency, the absorption curve of a homogeneous layer of the optimized foam with 24 mm thickness is calculated using theory of Biot and the equivalent fluid model. Since the frame acts as rigid above the decoupling frequency, the two models should be in agreement in the inertial regime. This comparison is shown in Figure 6. As expected, there is a significant discrepancy between the two models for frequencies much higher than the f_c. This confirms that the mass-spring effect noticed at 700 Hz is in the viscous regime.

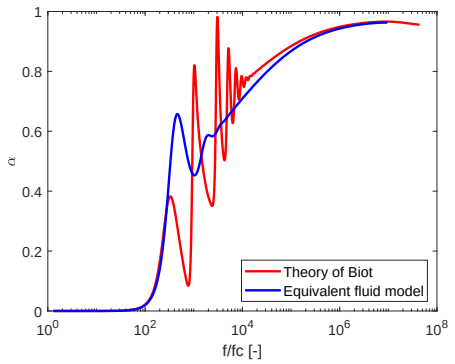

Figure 6: The absorption coefficient of a homogeneous layer of the optimized foam calculated using the theory of Biot and the equivalent fluid model.

4 Conclusions

In this paper, a perfect absorption coefficient is achieved at a single frequency in a meta-poro-elastic system below the decoupling frequency by exploiting the mass-spring effect. It is shown that embedding a mass inclusion in foams with specific material properties can lead to perfect absorption at tuned frequencies. In this study, only the inertial contribution of the inclusion is considered to ensure that the changes in the absorption behavior of the system are due to the mass-spring effect. An optimization routine is used to derive the material properties that magnify the viscous losses induced by the mass-spring effect. The feasibility of achieving broadband near-perfect or perfect absorption behavior is evaluated by considering a super-cell of the optimized foam with multiple inclusions such that a multi-degree-of-freedom mass-spring system can

be created. It is shown that the mass-spring effect is efficient in the viscous regime and it is important to use a correct criterion to identify the decoupling frequency. The commonly used definition of decoupling frequency, based on the porosity and the flow resisitivity of the foam, is valid for a wide range of materials, however, it is not accurate for foams with very short viscous characteristic length. On the other hand, the inverse quality factor, which corresponds to the amount of damped energy by the two longitudinal waves, seems to be a good indicator for the decoupling frequency.

Acknowledgements

The European Commission is gratefully acknowledged for their support of the VIPER research project (GA 675441) and the WIDEA project (GA 797034). The Research Fund KU Leuven is gratefully acknowledged for its support. The research of E. Deckers is funded by a grant from the Research Foundation – Flanders (FWO). This research was partially supported by Flanders Make, the strategic research centre for the manufacturing industry. The research of T. G. Zieliński and Ł. Jankowski is funded by the National Science Centre (NCN), Poland, under Grant Agreement No. 2015/19/B/ST8/03979.

References

[1] J.-P. Groby, A. Wirgin, L. De Ryck, W. Lauriks, R. P. Gilbert, and Y. S. Xu, "Acoustic response of a rigid-frame porous medium plate with a periodic set of inclusions," *J. Acoust. Soc. Am.*, vol. 126, no. 2, pp. 685–693, 2009.

[2] J.-P. Groby, O. Dazel, A. Duclos, L. Boeckx, and L. Kelders, "Enhancing the absorption coefficient of a backed rigid frame porous layer by embedding circular periodic inclusions," *J. Acoust. Soc. Am.*, vol. 130, no. 6, pp. 3771–3780, 2011.

[3] J.-F. Allard, O. Dazel, G. Gautier, J.-P. Groby, and W. Lauriks, "Prediction of sound reflection by corrugated porous surfaces," *J. Acoust. Soc. Am.*, vol. 129, p. 1696, 2011.

[4] T. Weisser, J.-P. Groby, O. Dazel, F. Gaultier, E. Deckers, S. Futatsugi, and L. Monteiro, "Acoustic behavior of a rigidly backed poroelastic layer with periodic resonant inclusions by a multiple scattering approach," *J. Acoust. Soc. Am.*, vol. 139, no. 2, pp. 617–629, 2016.

[5] T. G. Zieliński, "Modelling of poroelastic layers with mass implants improving acoustic absorption," in *Proceedings of ICA2007 – 19th International Congress on Acoustics, 2-7 September 2007, Madrid, Spain*, 2007.

[6] M. Kidner, C. Fuller, and B. Gardner, "Increase in transmission loss of single panels by addition of mass inclusions to a poro-elastic layer: Experimental investigation," *J. Sound Vib.*, vol. 294, pp. 466–472, jun 2006.

[7] S. Ahsani, E. Deckers, T. G. Zielinski, L. Jankowski, C. Claeys, and W. Desmet, "Absorption enhancement in poro-elastic materials by mass inclusion, exploiting the mass-spring effect," in *The proceedings of ECCOMAS SMART 2019*, 2019.

[8] S. Jonckheere, *Wave based and hybrid methodologies for vibro-acoustic simulation with complex damping treatments*. PhD thesis, KU Leuven, 2015.

[9] E. Deckers, S. Jonckheere, D. Vandepitte, and W. Desmet, "Modelling techniques for vibro-acoustic dynamics of poroelastic materials," *Arch. Computat. Methods. Eng.*, vol. 22, no. 2, pp. 183–236, 2015.

[10] C. Lagarrigue, J. P. Groby, O. Dazel, and V. Tournat, "Design of metaporous supercells by genetic algorithm for absorption optimization on a wide frequency band," *Appl. Acoust.*, vol. 102, pp. 49–54, 2016.

[11] P. M. Morse and K. U. Ingard, *Theoretical acoustics*. Princeton university press, 1986.

[12] M. A. Biot, "Theory of deformation of a porous viscoelastic anisotropic solid," *Journal of Applied physics*, vol. 27, no. 5, pp. 459–467, 1956.

[13] M. A. Biot, "Theory of propagation of elastic waves in a fluid-saturated porous solid. ii. higher frequency range," *The Journal of the acoustical Society of america*, vol. 28, no. 2, pp. 179–191, 1956.

[14] J. Allard and N. Atalla, *Propagation of sound in porous media: modelling sound absorbing materials. Second Edition*. John Wiley & Sons, 2009.

[15] D. L. Johnson, J. Koplik, and R. Dashen, "Theory of dynamic permeability and tortuosity in fluid-saturated porous media," *J. Fluid Mech.*, vol. 176, pp. 379–402, 1987.

[16] Y. Champoux and J.-F. Allard, "Dynamic tortuosity and bulk modulus in air-saturated porous media," *J. Appl. Phys.*, vol. 70, no. 4, pp. 1975–1979, 1991.

[17] O. Dazel, F. Sgard, F.-X. Becot, and N. Atalla, "Expressions of dissipated powers and stored energies in poroelastic media modeled by {u, U} and {u, P} formulations," *The Journal of the Acoustical Society of America*, vol. 123, no. 4, pp. 2054–2063, 2008.

[18] N. Atalla, R. Panneton, and P. Debergue, "A mixed displacement-pressure formulation for poroelastic materials," *J. Acoust. Soc. Am.*, vol. 104, p. 1444, 1998.

[19] N. Atalla, M. A. Hamdi, and R. Panneton, "Enhanced weak integral formulation for the mixed (u,p) poroelastic equations," *J. Acoust. Soc. Am.*, vol. 109, no. 6, pp. 3065–3068, 2002.

[20] P. Debergue, R. Panneton, and N. Atalla, "Boundary conditions for the weak formulation of the mixed (u, p) poroelasticity problem," *J. Acoust. Soc. Am.*, vol. 106, no. 5, pp. 2383–2390, 1999.

[21] J.-P. Groby, C. Lagarrigue, B. Brouard, O. Dazel, V. Tournat, and B. Nennig, "Using simple shape three-dimensional rigid inclusions to enhance porous layer absorption," *J. Acoust. Soc. Am.*, vol. 136, no. 3, pp. 1139–1148, 2014.

[22] M. Collet, M. Ouisse, M. Ruzzene, and M. N. Ichchou, "Floquet-Bloch decomposition for the computation of dispersion of two-dimensional periodic, damped mechanical systems," *Int. J. Solids Struct.*, vol. 48, no. 20, pp. 2837–2848, 2011.

[23] D. Magliacano, M. Ouisse, A. Khelif, S. De Rosa, F. Franco, N. Atalla, and M. Collet, "Computation of dispersion diagrams for periodic porous materials modeled as equivalent fluids," *Mechanical Systems and Signal Processing*, vol. 142, p. 106749, 08 2020.

[24] V. Torczon and M. W. Trosset, "From evolutionary operation to parallel direct search: Pattern search algorithms for numerical optimization," *Computing Science and Statistics*, pp. 396–401, 1998.

[25] P. S. Kurzeja and H. Steeb, "About the transition frequency in biot's theory," *J. Acoust. Soc. Am.*, vol. 131, no. 6, pp. EL454–EL460, 2012.